Ab initio study of the martensitic bcc-hcp transformation in iron

Mathias Ekman, Babak Sadigh, and Kristin Einarsdotter
Division of Theoretical Physics, Royal Institute of Technology, SE-100 44 Stockholm, Sweden

Peter Blaha
Institute for Technical Electrochemistry, TU Vienna, A-1060 Vienna, Austria
(Received 14 January 1998)

We present an extensive study of the pressure-induced bcc to hcp martensitic transformation in iron, using a spin-polarized full-potential total energy technique. The calculated pressure where the phases have equal enthalpies, 10.3 GPa, agrees well with the experimental value. Total energy surfaces as a function of the atomic displacements, which in the bcc phase correspond to the T_1 N-point phonon mode and a long-wavelength shear, are calculated for six different volumes. We observe that the bcc phase is thermodynamically unstable with respect to the hcp phase, long before it becomes dynamically unstable. The transition pressure at room temperature is estimated to approximately 50 GPa. We find that magnetism is the primary stabilizing mechanism of the bcc structure. Furthermore, we observe a sudden drop in the magnetic moment at a certain point in the transition path, which results in a discontinuous derivative in the energy surface. This is a clear signature of a first order ferromagnetic to nonmagnetic transition, responsible for the main part of the latent heat developed in this martensitic transformation. We also observe low-spin states at certain structures and pressures. Finally we employ Stoner theory to explain the behavior of the magnetism along the transition path. [S0163-1829(98)06030-5]

I. INTRODUCTION

There is strong experimental evidence that the Earth's core is essentially composed of iron or an iron-dominated alloy.[1,2] At pressures lower than about 0.2 GPa, the phase diagram of iron is reasonably well known[3,4] but the region of high temperatures and high pressures is still, despite recent experimental work,[5–8] highly uncertain. This includes the pressures (300–400 GPa) and the temperatures (4000–8000 K) which are characteristic of the interior of the Earth. Even the stable solid phase of the inner core of the Earth is not firmly established.

Theoretical attempts[9–12] have been made to understand the phase diagram of iron and there have been extensive studies performed on the Bain's path for a transition from the bcc to the fcc structure (using a c/a variation in a bct structure).[11–13] The most often proposed crystalline structure of the inner core is the nonmagnetic hexagonal phase (hcp)[2,14–18] although there are speculations concerning other phases, such as a magnetic bct phase.[11] Since it is well known[12] that the hcp structure is lower in energy than the fcc structure for pressures ranging from 0 to 400 GPa it is of considerable interest to study the bcc to hcp transition.

It is our ambition to perform a detailed study of the pressure-induced transition path from the ground-state of iron; ferromagnetic bcc to the suggested phase of the inner core, i.e., nonmagnetic hcp. This includes a full description of the variation of the ferromagnetic moment along the transition path. No calculations of the total energy (or enthalpy) of iron for a bcc to hcp transition path have, to our knowledge, yet been done.

Experimental work has shown that the bcc to hcp transition takes place at a pressure of 10–15 GPa, at room temperature, with a hysteresis that is characteristic of a martensitic phase transition.[19–21]

Despite considerable theoretical effort, the mechanism for such a martensitic phase transition (MPT) is still not clear. Cochran[22] and Anderson[23] formulated a soft-phonon model according to which the frequency of the relevant phonon branch should go to zero at the MPT. However, only a few systems show this behavior.[24] Krumhansl and Gooding[25] proposed a model based on the anharmonicity of an order parameter using a Landau-type expansion including fluctuations of the relevant order parameter. On the basis of such a model the fcc to bcc MPT in several metallic systems has been explored recently.[26,27] Another (fluctuationless) model, where the MPT is caused by defects, was suggested by Vul and Harmon.[28]

We use first-principles total energy calculations for iron to obtain the complete energy surface as a function of the transition path coordinates from the bcc to the hcp structure. The energy surface is determined for the volume corresponding to the transition pressure and for several higher as well as lower volumes. We also construct an enthalpy surface and a volume surface at the calculated transition pressure. These surfaces display in detail how the transition proceeds as pressure is applied. Besides this static information, the accurate energy surfaces can be fitted to empirical interatomic potentials which can then be used in future molecular dynamics simulations to study the dynamics of the transition. The ferromagnetic moments of the structures are carefully studied, both in a self-consistent spin-polarized (SCSP) scheme and in fixed spin-moment (FSM) calculations. The FSM results are used in a Stoner analysis, which allows us to locate possible ferromagnetic phases and the conditions for their emergence as a function of pressure. Together with the SCSP results, they complete the picture of how the magnetism de-

 © 1998 The American Physical Society

creases along the transition path from ferromagnetic bcc to nonmagnetic hcp iron, for different pressures.

This paper is organized as follows. In Sec. II, a brief description of the geometry of the transition is given. Sections III and IV contain the details of our calculations and calculated ground state properties of the bcc and hcp phases. In Sec. V we discuss the phonon instability and relate it to the electronic structure of bcc iron. Section VI presents the study of the transition path and the results in terms of surface plots for the transition energy, the enthalpy and the volume. In Sec. VII we study the variation of the magnetic moments along the transition path and discuss the development of the magnetism employing the Stoner model. We show that the bcc to hcp martensitic transition is a first-order magnetic phase transition which exhibits itself in a cusp (a discontinuous derivative) on the energy versus displacement plot and in a volume discontinuity. Furthermore, we show that the bcc phase is thermodynamically unstable with respect to the hcp phase long before it becomes dynamically unstable and that the subsequent instability is not primarily due to phonon softening but to the effect of pressure on the magnetism of iron.

II. STRUCTURAL MODEL

In order to describe the bcc-hcp martensitic transformation it is necessary to know which planes are transformed into each other. These crystallographic relations, established in 1934 by Burgers,[29] are described in compact form as

$$(100)_{\mathrm{bcc}} \| (001)_{\mathrm{hcp}}, [111]_{\mathrm{bcc}} \| [110]_{\mathrm{hcp}}. \tag{1}$$

The above relations can be achieved by a transformation scheme, involving two distortions. (i) Opposite displacement of adjacent $(110)_{\mathrm{bcc}}$ planes in the $[110]_{\mathrm{bcc}}$ direction which corresponds to the T_1 phonon mode at the N-point of the bcc Brillouin zone boundary. This displacement can be described by a parameter δ which is the relative amplitude of the phonon. (ii) Volume conserving shear deformation in the $[001]_{\mathrm{bcc}}$ direction, keeping the distance between the $(110)_{\mathrm{bcc}}$ planes unchanged. The shear can be characterized by a parameter θ, which is the angle between the two-body diagonals contained in the $(110)_{\mathrm{bcc}}$ plane.

In an explicit manner, the above transformation can be described on a c-based-centered lattice with lattice vectors: $[a/2,-b/2,0]$, $[a/2,b/2,0]$, and $[0,0,c]$, where the $[0,0,1]$ direction corresponds to the $[1,1,0]$ direction in bcc. The bcc lattice is then described by $a=a_{\mathrm{bcc}}$, $b=\sqrt{2}a_{\mathrm{bcc}}$, and $c=\sqrt{2}a_{\mathrm{bcc}}$ with atoms at $\mathbf{x}_1=(0,1/4,1/4)$ and $\mathbf{x}_2=(0,3/4,3/4)$. The phonon can be applied as $\mathbf{x}_1'=\mathbf{x}_1+(0,\delta,0)$ and $\mathbf{x}_2'=\mathbf{x}_2-(0,\delta,0)$ and the volume conserving shear can be written as

$$\begin{pmatrix} a' \\ b' \\ c' \end{pmatrix} = \begin{pmatrix} 1/\alpha & 0 & 0 \\ 0 & \alpha & 0 \\ 0 & 0 & 1 \end{pmatrix} \begin{pmatrix} a_{\mathrm{bcc}} \\ \sqrt{2}a_{\mathrm{bcc}} \\ \sqrt{2}a_{\mathrm{bcc}} \end{pmatrix}, \tag{2}$$

where $\alpha=[(1/\sqrt{2})\tan(\theta/2)]^{1/2}$. In these coordinates the bcc lattice corresponds to $\delta=0$, $\theta=109.47°$ and the hcp lattice to $\delta=1/12$ and $\theta=120°$. This transition path has earlier been used for the study of the same martensitic transition in Ba.[30,31] The hcp phase obtained upon transformation along this path has a c/a ratio of 1.57. This is not the ideal close packing ratio, but previous theoretical studies for iron[11,12] indicate that c/a variations have a small effect on the total energy.

TABLE I. Calculated and experimental values for the equilibrium volumes, bulk moduli, and T_1 N-point phonon frequency.

	V_0 [(a.u.)^3/atom)]		B_0 (GPa)		ν (THz)	
	LAPW	Expt.	LAPW	Expt.	LAPW	Expt.
bcc	78.15	79.51	185	172	5.22	4.53
hcp	68.94		263			

III. DETAILS OF CALCULATION

In the calculation of the electronic band structure energies, we used WIEN95,[32] a full-potential linearized augmented plane wave (FP-LAPW) method. The LAPW method divides the unit cell into nonoverlapping atomic spheres and an interstitial region. Inside the atomic spheres a linear combination of radial functions multiplied by spherical harmonics is used, and plane waves are used in the interstitial region. The solutions to the Kohn-Sham equations[33] are expanded in this combined basis set. The method is free of shape approximations to the charge density or the potential. The corrected tetrahedron method[34] was used for Brillouin zone integrations. The calculations were spin-polarized and the exchange and correlation contributions to the total energy were obtained within the generalized-gradient approximation (GGA) of Perdew and Wang.[35] Using GGA, and not just the local-spin-density-approximation (LSDA), is essential because within LSDA one finds for iron a nonmagnetic (NM) fcc ground state, in contrast to the experimentally found ferromagnetic (FM) bcc phase.

We used a $15\times15\times8$ **k**-point mesh, yielding 256 **k** points in the irreducible part of the Brillouin zone, for all structures. The muffin-tin radius was set to 2.0 a.u. and the product of the muffin-tin radius and the maximum reciprocal space vector $k_{\max}$, $R_{MT}k_{\max}$ was equal to 10. The maximum l value for the waves inside the atomic spheres, $l_{\max}$, and the largest **G** in the charge Fourier expansion, $G_{\max}$, was set to 10 and 14, respectively. The number of radial mesh points was 799. All total energy SCSP calculations were converged to within 0.05 mRy/atom.

IV. GROUND STATE PROPERTIES

Earlier theoretical calculations[11,12] predict the FM bcc iron to be the stable phase at ambient conditions while at higher pressures the NM hcp iron becomes energetically more favorable. For comparison with these studies, we performed calculations for the binding energies of the bcc and hcp iron structures. Values for the equilibrium volumes and the zero-pressure bulk moduli for the two phases are presented in Table I. The experimental magnetic moments of the bcc and hcp iron, $2.2\mu_B$ and $0.0\mu_B$ respectively, were correctly reproduced. The two structures have equal energies at the volume 70.3 a.u.^{3}. The thermodynamically stable phase is given by minimizing the *enthalpy* with respect to the

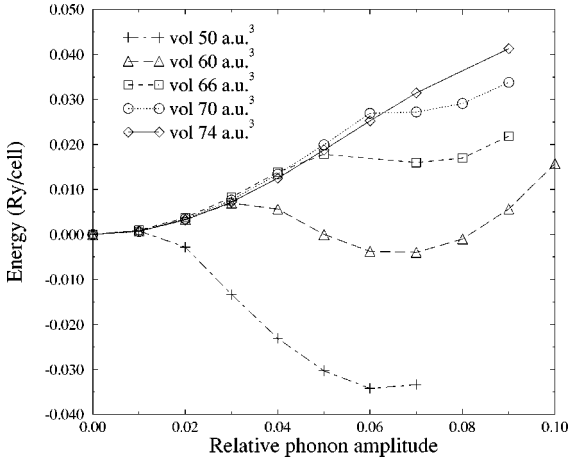

FIG. 1. The total energy vs the relative T_1 N-point phonon amplitude for five different volumes.

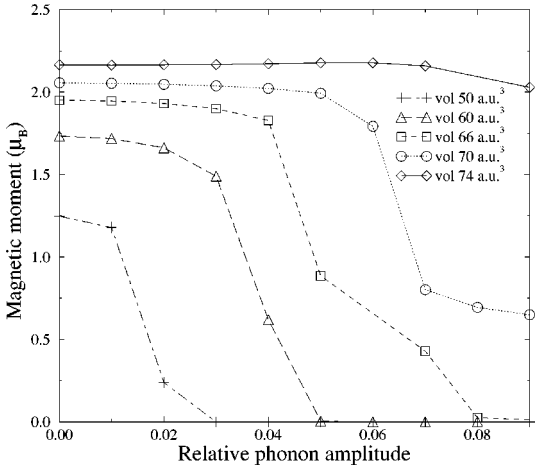

FIG. 2. The magnetic moment vs the relative T_1 N-point phonon amplitude for five different volumes.

state variables. Our calculation of the enthalpy as a function of the pressure yields a transition pressure of 10.3 GPa, in good agreement with the experimental[19,21] value, 10–15 GPa, and previous theoretical calculations.[11,12]

V. MECHANICAL INSTABILITY OF THE bcc PHASE

From the discussion in the previous section we expect a transition from the bcc to the hcp phase to take place when the applied pressure exceeds 10.3 GPa. However, before a transition can occur, the bcc phase must become dynamically unstable with respect to distortions which transform it to the hcp structure. The transition path studied in the present work involves two degrees of freedom, i.e., δ and θ. In this section we focus our attention on δ, i.e., the amplitude of the T_1 N-point phonon. The study of this phonon alone is an important first step for the understanding of the bcc-hcp transition since $\delta=1/12$ yields a nearly hexagonal phase.

Hence we performed total energy calculations for a set of distortions with $\delta\in[0.00,0.10]$ and $\theta=109.47°$ for five different volumes. The results are presented in Fig. 1. The experimental zone-boundary T_1 N-point phonon frequency has been measured[36–39] to 4.53 THz and compares well with our calculated 5.22 THz. A first important result of these calculations is that the pressure does not significantly affect the harmonic frequency of this mode. Analysis of the data shows a slight stiffening of the mode which abates with high pressure. The total energy versus phonon amplitude plot, cf. Fig. 1, is not a smooth double-well curve, but has a cusp. As the pressure is increased the cusp approaches the bcc phase ($\delta=0$), eventually making the bcc crystal unstable. It is also important to note that before the bcc phase becomes unstable, the energy of the sheared hcp phase is already lower than that of the bcc phase. Therefore, latent heat is developed during the transition, which indicates that it is of first order.

In Fig. 2 we present the magnetic moment, m, versus the relative phonon amplitude, δ, of the T_1 N-point phonon. The results for the magnetic moment of bcc iron as a function of pressure agree with previous studies.[11] Note that the position of the cusp in the total energy curve agrees well with the phonon amplitude where a sudden drop in the magnetic moment is observed. This is a feature of a magnetic first-order phase transition.

To study this issue further we performed FSM calculations for the volumes 70 a.u.^{3} with $m=0$ and 50 a.u.^{3} with $m=2.0\mu_B$. The results are shown in Fig. 3 together with the previous calculations where the spins were allowed to converge self-consistently. We observe that the bcc phase is unstable in the NM phase at the volume 70 a.u.^{3}, but that it can be stabilized at 50 a.u.^{3} with a magnetic moment of $2.0\mu_B$. This is consistent with the result presented in Fig. 1 and Fig. 2, which shows that the bcc phase becomes unstable because the ferromagnetism diminishes as the volume decreases.

Previous work[9] shows that the Bain's path from FM bcc to NM fcc also exhibits a cusp in the energy versus *c/a* curve where a magnetic first-order phase transition occurs. It is obvious from our FSM calculations that without the influence of magnetism, this instability would have occurred at a lower pressure. Hence, we conclude, in agreement with Ref. 10, that magnetism in bcc iron has a stabilizing effect. This scenario, where it is the effect of pressure on the magnetic moment that eventually causes the instability, is quite different from the results for Ba,[30] where the T_1 phonon softens as the pressure is increased.

We will now discuss the electronic origin of the pressured-induced instability in bcc iron. Figure 4(a) shows

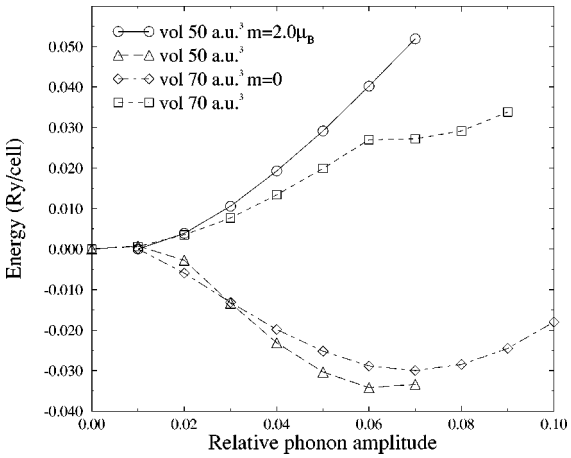

FIG. 3. The SCSP calculations for volumes 50 a.u.^{3} and 70 a.u.^{3} are shown together with FSM results for volume 70 a.u.^{3} with $m=0$ and volume 50 a.u.^{3} with $m=2.0\mu_B$.

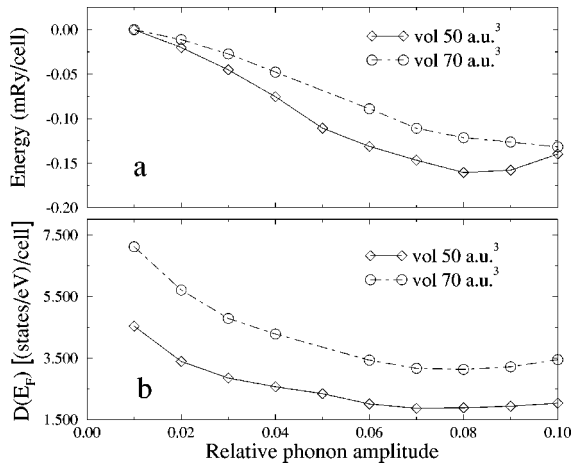

FIG. 4. (a) The valence-band energy vs the relative phonon amplitude for the NM bcc phase at volumes 50 a.u.^{3} and 70 a.u.^{3}. (b) The density of states at the Fermi level vs the relative phonon amplitude for the NM bcc phase at volumes 50 a.u.^{3} and 70 a.u.^{3}. Note that the bcc phase corresponds to phonon amplitude zero but that the hcp phase is not reached by the phonon alone.

the NM valence-band energy as a function of δ for the volumes 70 a.u.^{3} and 50 a.u.^{3}. We note that δ-distortion reduces the band energy of the bcc structure by $\approx$150 mRy at the volume 70 a.u.^{3} and $\approx$130 mRy at the volume 50 a.u.^{3}, which is about 3 to 4 times larger than is observed for the total energy (cf. Fig. 3). This is due to the fact that the decrease in the band energy is partly compensated by the increasing Madelung energy, which has its minimum at the undistorted structure. We nevertheless conclude that the instability of the NM bcc phase against δ distortions is to a large extent caused by the electronic band energy.

Inspection of the bcc density of states, $D(E)$, confirms what is to be expected for a transition metal in a high-symmetry phase with flat degenerate d-bands near the Fermi level E_{F}, i.e., $D(E)$ has a peak close to E_{F}. Such a state is energetically unfavorable. Its energy can be lowered in essentially two ways. (i) By lifting the degeneracies in the electronic energy bands through lattice distortions which reduces the symmetry of the crystal, hence lowering the number of electronic states at the Fermi level. This is illustrated in Fig. 4(b), where $D(E_{\mathrm{F}})$ of NM iron is plotted as a function of δ, for the volumes 70 a.u.^{3} and 50 a.u.^{3}. We see a clear decrease in $D(E_{\mathrm{F}})$, analogous to the reduction of the band energy, which is displayed in Fig. 4(a). (ii) By lifting the spin degeneracy and allowing for spin-polarization. This will lead to a splitting of the up and down spin bands, thus reducing $D(E_{\mathrm{F}})$ significantly.

It is a well-known fact that in bcc iron the latter scenario takes place, which is confirmed by our SCSP calculations. The spin-splitting which gives rise to magnetism thus stabilizes the bcc structure since the degenerate flat bands are no longer positioned near the Fermi level. Therefore there is no energy gain in lowering the symmetry through atomic displacements. However, we have already seen that at high pressures and for large enough distortions a cusp in energy occurs, corresponding to a sudden drop in the magnetic moment (cf. Figs. 1 and 2).

A qualitative physical interpretation can be given within the Stoner model, assuming slowly varying $D(E_F)$, as well as rigid shift of the up and down spin bands. The change in energy upon flipping the spins from the NM to the FM state then is

$$\Delta E(m) = \frac{1}{4}\frac{m^2}{D(E_{\mathrm{F}})}[1 - ID(E_{\mathrm{F}})], \tag{3}$$

where m is the magnetic moment and I is the Stoner parameter, which is a constant in this model. From Eq. (3) we see that the system is unstable towards FM ordering if

$$ID(E_{\mathrm{F}}) > 1, \tag{4}$$

which is the Stoner criterion. It is now clear that for large distortions, when $D(E_{\mathrm{F}})$ becomes small enough, the criterion for magnetic instability is no longer fulfilled which leads to a drop in the magnetic moment, followed by a cusp in the energy. The effect of pressure is essentially to enhance the overlap of the atomic wave functions, which in turn broadens the flat d-bands close to E_{F} and therefore lowers $D(E_{\mathrm{F}})$ [cf. Fig. 4(b)]. Smaller distortions are then needed to induce the transition from the FM to the NM state, hence the cusp in energy approaches the bcc phase.

The band model discussed in this section is of course crude but it gives an intuitive picture of the physics involved. In Sec. VII we will perform an improved analysis of our results within the framework of the Stoner theory. There we will allow for a varying Stoner parameter and the shape of the $D(E)$ near the Fermi level will be taken into account.

VI. TRANSITION DYNAMICS

To obtain the bcc-hcp phase transition path, we calculated the total energy on a two-dimensional grid of shear angles (θ) and relative phonon displacements (δ), for six different volumes. The energy surfaces were constructed using a fourth order polynomial fit to the energy in the θ direction and then connecting the curves linearly along the δ coordinate. Only three of the six energy surfaces are shown here. The energy surfaces can be divided into two connected regions, with extrema centered at the two stable high-symmetry phases. Where these regions meet, the energy has a cusp, similar to the one discussed in Sec. V. The cusp is the peak of the barrier separating the bcc and the hcp phases. A study of the variation of the magnetic moment in the (δ,θ) plane (cf. Fig. 8) suggests that the two regions are strongly influenced by the magnetic state of its high-symmetry structure. Hence the structures surrounding the bcc phase (bcc-related) are ferromagnetic with magnetic moments close that of the bcc phase, while the hcp-related ones are nonmagnetic. Clearly, the discontinuous change in the energy derivative at the boundary between the two regions is a signature of a magnetic first-order phase transition.

At the volume 74 a.u.^{3}, cf. Fig. 5, both phases are stable but the bcc structure has the lowest energy and the barrier between them is approximately 15 mRy/atom. With the application of pressure the energy difference between the bcc and hcp phases decreases, and the region of bcc-related structures shrinks and the cusp approaches the bcc phase, lowering the barrier between the phases. This agrees well with our observations in the previous section. At volume 70.3 a.u.^{3} where the bcc and hcp phases have equal energies,

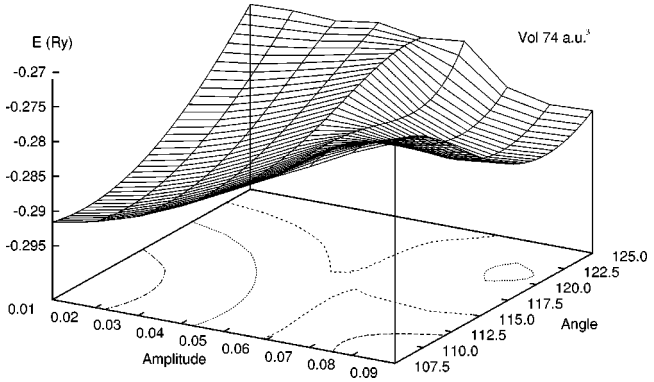

FIG. 5. The surface plot of the calculated total energy as a function of the relative atomic displacement corresponding to the T_1 N-point phonon mode and the angle of the shear motion at volume 74 a.u.^{3}. The coordinates for the bcc and hcp phase are $(\delta,\theta)=(0,109.5)$ and $(\delta,\theta)=(1/12,120)$, respectively. The contours, with spacing 5 mRy, are guides to the eye.

cf. Fig. 6, there is still a barrier of about 9 mRy/atom between them. At the smallest volume, 60 a.u.^{3} (Fig. 7), which is equivalent to a pressure of 90 GPa for the bcc phase, the barrier is about 3 mRy/atom which corresponds to a temperature of 500 K.

As we study the magnetic moment for large δ and small θ at volume 70 a.u.^{3}, cf. Fig. 8, where we find states with intermediate magnetic moments of about $1\mu_B$. Thus, in addition to the FM to NM transition we have discussed so far, we see evidence of magnetic transitions from high-spin to low-spin states. It is interesting to describe the changes in the magnetic moment from a structural point of view, relating them to the change in coordination number. In the bcc phase, iron has 8 nearest and 4 next-nearest neighbors and a large moment. When the coordination number changes to approximately $10+2$, a stabilization of a moment of about $1\mu_B$ is possible, while 12 nearest neighbors leads to a NM phase. Neighbors within a range of about 5.0–5.1 a.u. can be considered to be in the first shell, although the distance changes slightly with volume or extreme short (long) nearest neighbor distances in some distorted structures. In the next section we will give a more quantitative description of the magnetic features discussed here.

We have seen evidence that the martensitic bcc-hcp transition is a first-order magnetic phase transition in which we

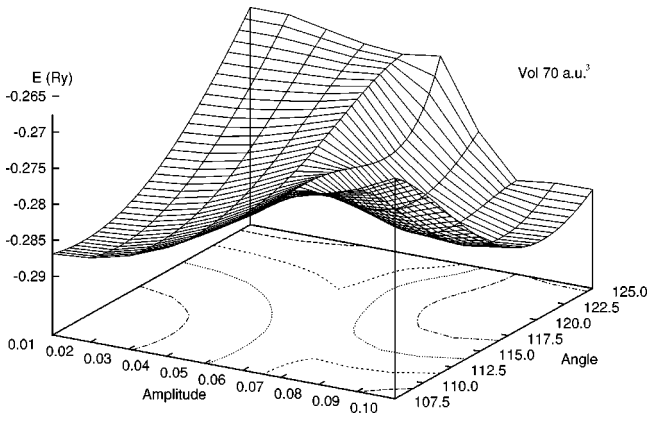

FIG. 6. As in Fig. 5, for $V=70$ a.u.^{3}.

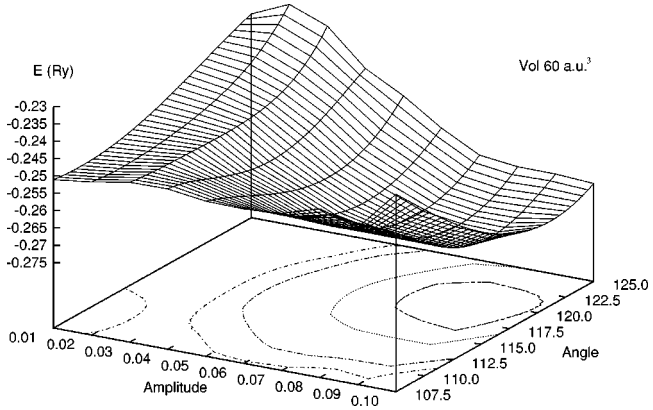

FIG. 7. As in Fig. 5, for $V=60$ a.u.^{3}.

expect a volume discontinuity at the point in the path where the magnetism drops, i.e., at the position of the cusp in the energy. This volume change will affect the enthalpy which is the quantity that determines the phase stability at 0 K. Since we have calculated the total energy for every transition coordinate (δ,θ) as a function of the six volumes, an enthalpy surface can be contructed. Fitting a third order polynomial to the energy as a function of the volume, we calculate the curvature, i.e., the pressure. Keeping the pressure fixed and solving for the energy and volume, we thus obtain the enthalpy $H(P)$. This procedure is repeated for every (δ,θ) grid point, resulting in

$$H(P,\delta,\theta)=E(P,\delta,\theta)+PV(P,\delta,\theta). \tag{5}$$

Figure 9 shows the enthalpy as a function of the transition coordinates at 10.3 GPa. At this pressure the *enthalpy* barrier between the two phases is approximately 8 mRy/atom. Studying enthalpy surfaces at higher pressures reveals that room temperature excitations enables a transition at 50 GPa. As expected, the enthalpy surface displays a lowering of the

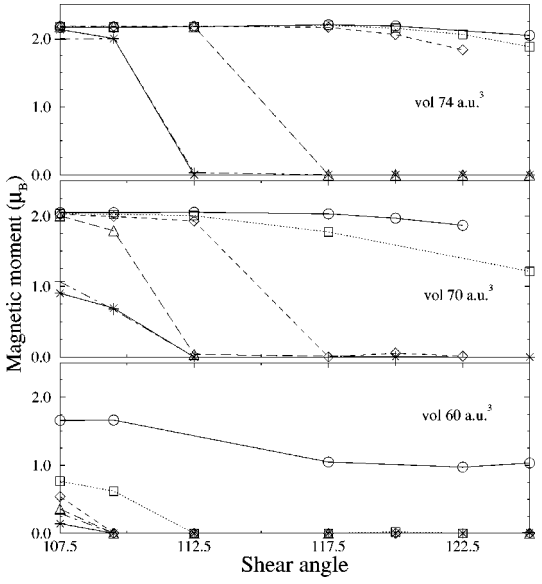

FIG. 8. Magnetic moments at three different volumes with varying shear angle θ for relative phonon amplitudes δ: 0.02 (circle), 0.04 (square), 0.05 (diamond), 0.06 (triangle), 0.08 (plus), and 0.10 (star).

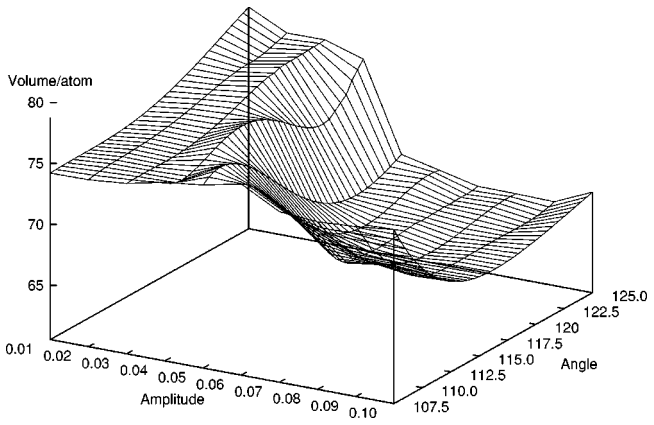

FIG. 9. The surface plot of the enthalpy at the pressure 10.3 GPa, as a function of the relative phonon amplitude and shear angle. The coordinates for the bcc and hcp phase are $(\delta,\theta)=(0,109.5)$ and $(\delta,\theta)=(1/12,120)$, respectively. The zero point of the enthalpy scale is set to -2546 Ry. The contours are guides to the eye.

barrier between the two phases due to the volume discontinuity. Also importantly, the enthalpy surface plot confirms that we find the minimum enthalpy path between the bcc phase and the hcp phase by coupling the phonon with the shearing of the lattice.

In calculating the enthalpy surface we also obtained the volume as a function of the transition coordinates. Figure 10 shows the volume surface for the pressure 10.3 GPa. We observe that for a certain displacement $(0.04<\delta<0.05)$ agreeing with the position of the magnetic transition, there is a sudden drop in the volume, compatible with a first-order phase transition.

Revisiting the Stoner model discussed in the previous section, we can give a qualitative explanation for this behavior. By assuming a volume-independent Stoner parameter I and a d-band width that varies inversely with the volume to the 5/3 power,[40] we get directly from Eq. (3) that

$$P_{\mathrm{mag}}V=\frac{5}{12}\frac{m^2}{D(E_{\mathrm{F}})}. \tag{6}$$

Hence at a magnetic transition when m suddenly drops to zero, the magnetic pressure vanishes. Consequently the volume of a system under a fixed pressure, which undergoes an FM to NM transition, shrinks significantly.

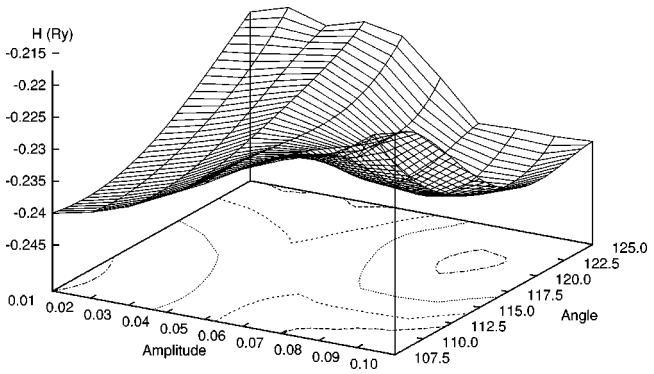

FIG. 10. The surface plot of the volume at the pressure 10.3 GPa as a function of the relative phonon amplitude and shear angle. The coordinates for the bcc and hcp phase are $(\delta,\theta)=(0,109.5)$ and $(\delta,\theta)=(1/12,120)$, respectively. The volume is in a.u.^{3}/atom.

VII. ITINERANT-ELECTRON MAGNETISM

In the previous section, we discussed the behavior of the magnetism along the transition path. We saw that structures near the bcc phase are very stable high-spin states, with magnetic moments of approximately $2.0\mu_B-2.2\mu_B$, even at very high pressures. However, for certain distortions a magnetic transition takes place, involving a rapid drop of the magnetic moment which, close to the hcp structure, results in a NM final state. At volume 70 a.u.^{3}, there is a pronounced low-spin of approximately $1.0\mu_B$ for large δ and small θ. This well-defined low-spin state splits up as we increase the pressure.

In this section we wish to perform a detailed analysis of the FM behavior of iron along the bcc-to-hcp transition path by employing the Stoner theory on our self-consistent band calculations. This allows us to locate possible FM phases and find the conditions for their emergence. We define the difference between the number of spin-up and the spin-down electrons as n_m,

$$n_m=n_{\mathrm{up}}-n_{\mathrm{dn}}. \tag{7}$$

In the Stoner theory, the change in energy upon forming an FM state, with a given $m=n_m\mu_B$, is written as[41]

$$\Delta E(n_m,V)=\frac{1}{2}\int_0^{n_m}\frac{n_m{}'}{\overline{D}(n_m{}',V)}dn_m'-\frac{1}{4}I(n_m,V){n_m}^2, \tag{8}$$

where the first term is the kinetic contribution from flipping $n_m/2$ spin-down electrons into the spin-up band and the second term is the exchange energy. The average density of states appearing in the kinetic term is defined as

$$\overline{D}(n_m,V)=\frac{n_m}{E_F^{\mathrm{up}}-E_F^{\mathrm{dn}}}, \tag{9}$$

where E_F^{up} (E_F^{dn}) is the Fermi level of the spin-up (down) band as found from the rigid-subband shift. The Stoner parameter I is often treated as a constant which makes it possible to calculate the FM contribution to the total energy using only NM results. The Stoner parameter is then obtained from linear-response theory.[42] However, earlier work[9,41] has shown that I depends on the volume as well as the magnetic moment. We investigated this dependence for the bcc and two distorted structures by extensive FSM calculations. Due to the small energy differences involved, these calculations were converged to within 0.05 mRy/atom. As proposed in Ref. 41 we used the FSM results to calculate $\Delta E(n_m,V)$, which yields I as a function of n_m. Minimizing $\Delta E(n_m,V)$ with respect to n_m yields, apart from the trivial solution, $n_m=0$, the Stoner criterion of a possible FM state,

$$\overline{D}(n_m,V)\left[I(n_m,V)+\frac{1}{2}n_m I_{n_m}{}'(n_m,V)\right]=1. \tag{10}$$

If I is independent of n_m we get the usual Stoner criterion for ferromagnetism [Eq. (4)]. The FM state given by Eq. (10) is

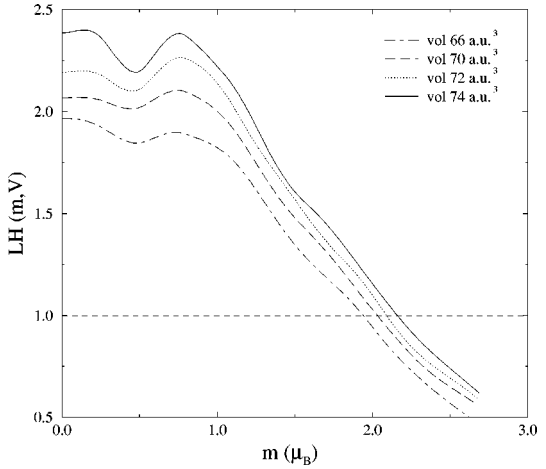

FIG. 11. The left hand side of Eq. (10), LH(m,V), for bcc at different volumes.

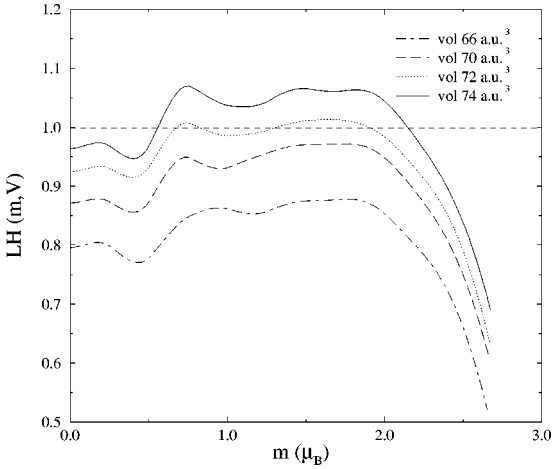

FIG. 13. The left hand side of Eq. (10), LH(m,V), for the phase with $\delta=0.06$ and $\theta=112.5°$.

metastable if $(\partial^2/\partial {n_m}^2)\,\Delta E(n_m,V)>0$, which is equivalent to a negative derivative of the left hand side of Eq. (10). From Eq. (8), using the fact that $\overline{D}(0,V)=D(E_F,V)$, we also obtain an expression for $I(0,V)$,

$$I(0,V)=\frac{1}{D(E_F,V)}-2\frac{\partial^2}{\partial {n_m}^2}\Delta E(n_m,V)\bigg|_{n_m=0}. \quad (11)$$

From Eq. (11) we observe that the NM state, $n_m=0$, is metastable if $I(0,V)D(E_F,V)<1$. Note that for $n_m=0$, the left hand side of Eq. (10) reduces to $I(0,V)D(E_F,V)$.

Figures 11–13 show the left hand side of Eq. (10), LH(m,V), as a function of m for the bcc phase, a nearly hexagonal structure and an intermediate structure for four different volumes ranging from 74 to 66 a.u.^{3}. We find that although the curves are shifted due to the volume change, the shape of the curves is not much affected. $I(n_m,V)$ and $\overline{D}(n_m,V)$ also exhibit this behavior, separately. This is important since it makes it possible to predict the emergence of different FM states (stable, unstable, and metastable) as pressure is applied to the crystal. Moreover, it was evident from our calculations that it is crucial to let I vary with m to get the correct low-spin states. These results are in agreement with previous studies.[41]

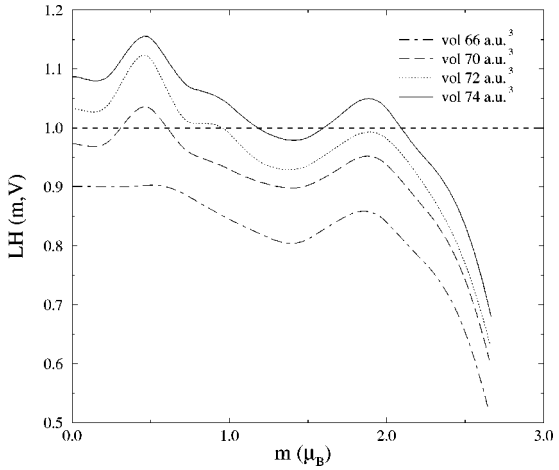

FIG. 12. The left hand side of Eq. 10, LH(m,V), for the phase with $\delta=0.08$ and $\theta=109.5°$.

Figure 11 shows the development of the FM state for the bcc structure as the volume is reduced. Because of the smooth monotonic behavior of the curve, the magnetic moment of the bcc phase will decrease slowly as pressure is applied until the magnetic moment reaches approximately $m=1.0\mu_B$ where the curve flattens out. At this point the magnetic moment of the FM state will decrease more rapidly and eventually bcc iron will transform into hcp structure, according to our conclusions in Sec. V. From the SCSP calculations we obtained, for the volume 50 a.u.^{3}, a nearly unstable state with magnetic moment of $1.25\mu_B$. This agrees very well with the Stoner analysis.

Quite a different picture is displayed in Figs. 12 and 13 where a more complicated dependence of m allows for an abrupter development of the FM state as well as the occurrence of low-spin states is observed in these structures. The curves in Fig. 12, representing the structure ($\delta=0.08$, $\theta=109.5°$), show an increasing trend with decreasing magnetic moment m, which means that a FM state will remain for moderate pressure. At the volume 74 a.u.^{3} there are three solutions to Eq. (10). A negative derivative at $m=2.1\mu_B$ indicates a metastable state, which is identified as the stable one because the state is also seen in Fig. 8. The state at $m=1.5\mu_B$ is unstable since the derivative is positive, and the third solution is a metastable low-spin state at $m=1.2\mu_B$. As pressure is slightly increased, the high-spin solution disappears and at volume 72 a.u.^{3} there is only one stable FM state at $m=1.0\mu_B$. At the lower volume 70 a.u.^{3} the NM state is metastable since $I(0,V)D(E_F,V)<1$. However, the FM state at $m=0.6\mu_B$ is the stable state as that state was also obtained in the SCSP calculations; see Fig. 8.

In Fig. 13 an intermediate structure ($\delta=0.06$, $\theta=112.5°$) is shown. The curves tend to decrease for small m, which results in a rapidly disappearing FM state as pressure is applied. At the volume 74 a.u.^{3} we find a metastable NM state and a FM state at $m=2.1\mu_B$. The latter is stable as it agrees with the results in Fig. 8. Already at the volume 70 a.u.^{3}, the NM state is the only stable one, as can also be seen in Fig. 8.

VIII. CONCLUSIONS

In conclusion, we used first-principles total energy calculations to study the pressure-induced bcc-hcp phase transition in iron. The transition path between the two phases is completely mapped out and described in terms of total energy (and enthalpy) versus two independent coordinates, one phonon amplitude and one shear. An important result from our investigation is that iron remains stable at low temperatures against these distortions until the magnetic moment is sufficiently suppressed by the pressure. Unlike studies of this path from bcc to hcp in other elements[30,31] where the phonon softens as pressure is increased, the T_1 N-point phonon in iron shows no such behavior; in fact it stiffens very slightly. Furthermore, we observe several indications that the actual transition is of first-order: latent heat is developed, and there is a discontinuous derivative in the total energy versus the phonon amplitude at the point where the magnetism drops. Simultaneously the volume, as a function of the transition coordinates, displays a similar sudden decrease. According to our results bcc iron would remain dynamically stable at low temperatures with respect to phonon displacements, as well as shear deformations, for all pressures considered in this study. The experimental transition pressure is 10.3 GPa, which agrees with the calculated pressure where the two phases have equal enthalpies. At this pressure our enthalpy surface still shows a pronounced barrier between the two phases. However, it is not possible to make a direct comparison between our calculations and room temperature experiments because of the entropy term, included in the free energy, which in this case consists not only of a vibrational and an electronic part but also a magnetic part. The magnetic entropy could contribute to a lowering of the bcc phase relative to the hcp phase phase, which in turn would increase the critical driving force for nucleation.[43–45] Another possibility is that the ground state of the intermediate structures could involve more complicated magnetic structures, for example, spin spirales. A lower energy (enthalpy) for the intermediate structures would lower the barrier between the phases. In fact, we have observed that the antiferromagnetic solution gives a lower energy than the nonmagnetic and ferromagnetic ones for the intermediate structures at volumes larger than 70.3 a.u.^{3}. However, at volume 70.3 a.u.^{3} the *energy* barrier is reduced by 1.0 mRy/atom but at higher pressures the decrease of the barrier lessens. The volume at the top of the *enthalpy* barrier (see Fig. 10) is about 70 a.u.^{3}, which means that the *enthalpy* barrier is slightly decreased by allowing for antiferromagnetism during the transition from bcc to hcp iron.

Furthermore, we are able to explain the abrupt changes in magnetic moment and low-spin occurrences along the transition path by using the Stoner model. The Stoner analysis also supports our observations of the development of magnetism in bcc iron under pressure.

Finally, we conclude that the thermodynamic conditions for a phase transition from bcc to hcp iron will eventually be fulfilled, at a sufficient temperature and pressure.

ACKNOWLEDGMENTS

The authors want to thank G. Grimvall for valuable comments on the paper. This work was supported by the Swedish research foundation SSF. P.B. was supported by the Austrian Science Foundation Project No. P10847.

[1] F. Birch, J. Geophys. Res. **57**, 227 (1952).
[2] O. L. Anderson, Nature (London) **314**, 407 (1985).
[3] A. F. Guillermet and P. Gustafson, High Temp. High Press. **16**, 591 (1984).
[4] R. Boehler, Geophys. Res. Lett. **13**, 1153 (1986).
[5] Q. Williams, R. Jeanloz, J. Bass, B. Svendsen, and T. J. Ahrens, Science **236**, 181 (1987).
[6] R. Boehler, Nature (London) **363**, 534 (1993).
[7] S. K. Saxena, G. Shen, and P. Lazor, Science **260**, 1312 (1993).
[8] J. M. Brown and R. G. Mcqueen, J. Geophys. Res. **91**, 7485 (1986); C. S. Yoo, N. C. Holmes, M. Ross, D. J. Webb, and C. Pike, Phys. Rev. Lett. **70**, 3931 (1993).
[9] G. L. Krasko and G. B. Olson, Phys. Rev. B **40**, 11 536 (1989).
[10] H. Hasegawa and D. G. Pettifor, Phys. Rev. Lett. **50**, 130 (1983).
[11] P. Söderlind, J. A. Moriarty, and J. M. Willis, Phys. Rev. B **53**, 14 063 (1996).
[12] L. Stixrude, R. E. Cohen, and D. J. Singh, Phys. Rev. B **50**, 6442 (1994).
[13] L. Stixrude, R. E. Cohen, and D. J. Singh, Geophys. Res. Lett. **22**, 125 (1995).
[14] O. L. Anderson, Geophys. J. R. Astron. Soc. **84**, 561 (1986).
[15] J. Brown and R. McQueen, J. Geophys. Res. **91**, 7485 (1986).
[16] Q. Williams, Science **236**, 181 (1987).
[17] M. Ross, D. Young, and R. Grover, J. Geophys. Res. **95**, 21 713 (1990).
[18] C. S. Yoo, J. Akella, A. J. Campbell, H. K. Mao, and R. J. Hemley, Science **270**, 1473 (1995).
[19] A. P. Jephoat, H. K. Mao, and P. M. Bell, J. Geophys. Res. **91**, 4677 (1986).
[20] W. A. Bassett and E. Huang, Science **238**, 780 (1987).
[21] R. D. Taylor and M. P. Pasternak, J. Appl. Phys. **69**, 6126 (1991).
[22] W. Cochran, Adv. Phys. **9**, 387 (1960).
[23] P. W. Anderson, in *Fizika Dielectrikov*, edited by G. I. Skanzvi (Akad. Nauk S.S.S.R. Fizicheskii Inst. im P. N. Lebedeva, Moscow, 1960).
[24] J. A. Krumhansl, Solid State Commun. **48**, 251 (1982).
[25] J. A. Krumhansl and R. J. Gooding, Phys. Rev. B **39**, 3047 (1989).
[26] V. L. Sliwko, P. Mohn, K. Schwarz, and P. Blaha, J. Phys.: Condens. Matter **8**, 799 (1996).
[27] P. Mohn, K. Schwarz, and P. Blaha, J. Phys.: Condens. Matter **8**, 817 (1996).
[28] D. A. Vul and B. N. Harmon, Phys. Rev. B **48**, 6880 (1993).
[29] W. G. Burgers, Physica (The Hague) **1**, 561 (1934); A. Nagasawa, N. Nakanishi, and K. Enami, Philos. Mag. A **43**, 1345 (1981).
[30] Y. Chen, K. M. Ho, and B. N. Harmon, Phys. Rev. B **37**, 283 (1988).
[31] B. N. Harmon, in *Statics and Dynamics of Alloy Phase Transformations*, edited by P. E. Turchi and A. Gonis (Plenum Press, New York, 1994), p. 421.

[32] P. Blaha, K. Schwarz, P. Dufek, and R. Augustyn, WIEN95, Technical University of Vienna, 1995. [Improved and updated Unix version of the original copyrighted WIEN-code, which was published by P. Blaha, K. Schwarz, P. Sorantin, and S. B. Trickey, Comput. Phys. Commun. **59**, 399 (1990).]

[33] P. Hohenberg and W. Kohn, Phys. Rev. **136**, B864 (1964).

[34] P. E. Blöchl, Phys. Rev. B **49**, 16 223 (1994).

[35] J. P. Perdew, J. A. Chevary, S. H. Vosko, K. A. Jackson, M. R. Pederson, D. J. Singh, and C. Fiolhais, Phys. Rev. B **46**, 6671 (1992).

[36] V. J. Minkiewicz, G. Shirane, and R. Nathans, Phys. Rev. **162**, 528 (1967).

[37] B. N. Brockhouse, H. E. Abon-Helal, and E. D. Hallman, Solid State Commun. **5**, 211 (1967).

[38] C. Van Dijk and J. Bergsma, *Neutron Inelastic Scattering* (IAEA, Vienna, 1968), Vol. 1, p. 233.

[39] W. Van Dingenen and S. Hautecler, Physica (Amsterdam) **37**, 603 (1967).

[40] V. Heine, Phys. Rev. **153**, 673 (1967).

[41] P. M. Marcus and V. L. Moruzzi, Phys. Rev. B **38**, 6949 (1988).

[42] J. F. Janak, Phys. Rev. B **16**, 255 (1977).

[43] G. B. Olson and M. Cohen, in Proceedings of the International Conference on Martensitic Transformations (ICOMAT-82) [J. Phys. (Paris), Colloq. **43**, C4-75 (1982)].

[44] G. B. Olson and M. Cohen, in *Proceedings of the International Conference on Solid-Solid Phase Transformations*, edited by H. I. Aaronson (TMS-AIME, Warrendale, PA, 1982), p. 1145.

[45] G. B. Olson, *Proceedings of the International Conference on Martensitic Transformations* (ICOMAT-86) (Japan Institute of Metals, Miyagi, 1987), p. 25.